Soil Biology and Biochemistry 173 (2022) 108803

Contents lists available at ScienceDirect

Soil Biology and Biochemistry

journal homepage: www.elsevier.com/locate/soilbio

Microbe-iron interactions control lignin decomposition in soil

Cuijuan Liao [a,1], Wenjuan Huang [b,1], Jon Wells [c], Ruiying Zhao [d], Keanan Allen [c], Enqing Hou [e], Xin Huang [c], Han Qiu [f], Feng Tao [a], Lifen Jiang [c], Maricar Aguilos [g], Lin Lin [a], Xiaomeng Huang [a,**], Yiqi Luo [h,*]

[a] Department of Earth System Science, Ministry of Education Key Laboratory for Earth System Modeling, Institute for Global Change Studies, Tsinghua University, Beijing, China
[b] Department of Ecology, Evolution, and Organismal Biology, Iowa State University, Ames, IA, USA
[c] Center for Ecosystem Sciences and Society, Northern Arizona University, Flagstaff, AZ, USA
[d] College of Environmental and Resource Sciences, Zhejiang University, Hangzhou, China
[e] Key Laboratory of Vegetation Restoration and Management of Degraded Ecosystems, South China Botanical Garden, Chinese Academy of Sciences, Guangzhou, China
[f] Atmospheric Sciences and Global Change Division, Pacific Northwest National Laboratory, Richland, WA, USA
[g] Department of Forestry and Environmental Resources, North Carolina State University, Raleigh, NC, USA
[h] School of Integrative Plant Science, Cornell University, Ithaca, NY, 14853, USA

ARTICLE INFO

Keywords:
Lignin decomposition
Microbial model
Mineral associated organic matters
Iron redox
Data assimilation

ABSTRACT

Lignin decomposition is critically linked to terrestrial carbon (C) cycle due to the enormous C mass of lignin and its importance in controlling overall rates of litter decomposition. Interactions between lignin and iron (Fe) minerals have been increasingly recognized as key mediators of lignin decomposition in experimental studies. However, we still lack a quantitative understanding of how Fe minerals interact with microbes to control lignin decomposition. Here, we leveraged experimental results from an incubation of Fe-rich soil, in which lignin decomposition rates were measured at aerobic conditions after four levels of pre-treated O_2 availability, to examine microbe-Fe (MiFe) interactions in lignin decomposition with a MiFe model. We quantified how Fe redox cycling interacted with microbial activities to control lignin decomposition via data-model integration. Our results showed that the MiFe model with time-dependent growth and mortality functions better represented CO_2 release from lignin decomposition (R^2 ranging from 0.96 to 0.97) than models assuming either first-order or Michaelis-Menten kinetics. Reduction of Fe(III) to Fe(II) after pre-treatments with lower O_2 availability stimulated the Fenton reaction to break down macro-molecular lignin into small molecules available to microbes. The small molecules of lignin and necromass bounded with oxidized Fe and were protected from decomposition. After 1-year incubation, the model implied that most of C stabilized with Fe minerals was derived from small molecular lignin C. Our quantitative analysis of microbe-Fe interactions sheds new light on lignin decomposition and preservation and helps improve model prediction of soil C persistence under global change.

1. Introduction

Lignin is one of the most abundant plant-derived organic substances in the terrestrial ecosystems (Boerjan et al., 2003), and its decomposition is critically linked to soil carbon (C) input and persistence. Lignin has long been recognized to limit overall decomposition rate of plant litter due to its perceived biochemical recalcitrance relative to other organic constituents (Talbot and Treseder, 2012). Accordingly, lignin plays a critical role in litter and soil organic C (SOC) decomposition (Parton et al., 1987; Izaurralde et al., 2006). However, a new paradigm of SOC research has challenged the notion and posits that lignin can decompose faster than SOC as a whole (Amelung et al., 2008; Thevenot et al., 2010). Most of the previous studies suggested that lignin decomposition is primarily controlled by fungi and largely regulated by litter chemical properties. Recent work has pointed to the importance of interactions between soil minerals and lignin decomposition to partially

* Corresponding author.
** Corresponding author.
E-mail addresses: hxm@tsinghua.edu.cn (X. Huang), yl2735@cornell.edu (Y. Luo).
[1] The authors contributed equally to this study.

https://doi.org/10.1016/j.soilbio.2022.108803
Received 6 May 2022; Received in revised form 5 August 2022; Accepted 6 August 2022
Available online 12 August 2022

reconcile these old and new paradigms (Huang et al., 2019). Yet, fundamental processes that control lignin decomposition are to be understood for evaluating these competing conceptual models. Therefore, it is imperative to develop a generalizable framework to quantify the role of mineral-microbe interactions in lignin decomposition and SOC persistence.

Interactions of lignin and geochemical context, such as iron (Fe) minerals, have been increasingly recognized as key controllers for lignin decomposition (Hall et al., 2015, 2016). Reactive Fe minerals critically influence soil C dynamics through both biotic and abiotic processes (Weber et al., 2006; Kleber et al., 2015). Iron oxides can preferentially associate with aromatic lignin constituents via sorption and coprecipitation to protect lignin C from microbial attack, relative to other organic compounds (Kramer et al., 2012; Riedel et al., 2013). Besides the extracellular oxidative enzymes that are generally considered to break down lignin, reactive oxygen species such as hydroxyl radical generated via Fe redox cycling, known as the Fenton reaction (Hall and Silver, 2013; Hall et al., 2015), can cleave the relatively stable ether bonds of lignin (Wood, 1994; Hammel et al., 2002). Once lignin is depolymerized by these abiotic mechanisms, the lower molecular weight lignin fragments in principle could be readily metabolized by many bacteria in addition to fungi (Cotrufo et al., 2013). Together, Fe minerals exert dual impacts on lignin decomposition: protection of lignin-derived C by Fe oxides (Riedel et al., 2013; Hall et al., 2016; Coward et al., 2018) versus stimulation of lignin decomposition by reactive oxygen species produced via Fe redox cycling in fluctuating redox environments (Hall et al., 2015; Calabrese and Porporato, 2019; Huang et al., 2019).

Although mineral-microbe interactions have been widely understood to control lignin decomposition (Ginn et al., 2017; Calabrese and Porporato, 2019; Zheng et al., 2019; Huang et al., 2021), we still lack a generalizable framework to quantify these interactions that help estimate fates of lignin C and quantify contribution of lignin to SOC persistence. To develop the framework, we need comprehensive data sets to test alternative models regarding the role of mineral-microbe interactions. The study by Huang et al. (2019) employed a C stable isotope approach to distinguish the source of respired CO_2 and applied a single anaerobic event of varying duration to generate differences in Fe (II) at the beginning of the incubation. The data set includes high frequent measurements of lignin decomposition over ~1-yr incubation period (Huang et al., 2019). Interestingly, lignin decomposition rates reached different peaks several months after redox pre-treatments, which may indicate the strong interactions of Fe and lignin. The observed non-linear patterns clearly did not follow traditional first-order kinetics, which has been widely used to describe decomposition of litter and SOC (Parton et al., 1993; Bondeau et al., 2007; Adair et al., 2008; Clark et al., 2011; Koven et al., 2013). Sufficient incubation time and intensive observation data provide strong support for the construction and theoretical analysis of a new framework for lignin decomposition. Indeed, the pattern of lignin decomposition reported in Huang et al. (2019) was also observed in many other soils (Hall et al., 2020). Thus, a framework that is developed based on the data set in Huang et al. (2019) is likely to be applicable to other studies on lignin decomposition, especially in Fe-rich soils.

This study reveals likely mechanisms underlying lignin decomposition via microbe-Fe interactions based on a data-model synthesis of results from an experiment published by Huang et al. (2019). We first evaluated alternative mechanisms as expressed in process-based models, such as first-order kinetics in a multi-pool model, microbially mediated reaction in a Michaelis-Menten model, and microbe-Fe-mediated lignin decomposition as in a microbe-Fe interaction (MiFe) Model. The MiFe model incorporates Fe-mediated breakdown of macromolecular to small molecular lignin C via the Fenton reaction, microbial decomposition of small molecular lignin C, and protection of lignin C via Fe association (Fig. 1). Our evaluations indicated that neither the classical three-pool, first-order kinetics model nor the Michaelis-Menten model well represents the observed patterns of lignin decomposition in Huang et al. (2019) (Fig. 2). In contrast, our new MiFe model better reproduced the observed data (Fig. 2), and was the primary focus of this study. We interpreted modeling results to examine possible key controlling mechanisms and fates of lignin C in soil.

2. Materials and methods

2.1. Incubation data

The data used in this study were from an incubation study by Huang et al. (2019). In that incubation study, soil was sampled from an upland valley in a perhumid tropical forest near the El Verde field station of the Luquillo Experimental Forest (18°17′N, 65°47′W), Puerto Rico. This soil is an Oxisol developed from basaltic to andesitic volcaniclastic sediments (pH = 5.03). Soil organic carbon at 0–10 cm measured 44.8 mg g^{-1}, and soil nitrogen was 4.1 mg g^{-1}. The soil at 0–10 cm had 10% sand, 53% silt and 37% of clay. Information about soil sampling, the experimental design of applying C isotope-labeled lignin and high-frequency isotope measurements of lignin decomposition to CO_2 were described in detail in Huang et al. (2019). In general, Huang et al. (2019) amended

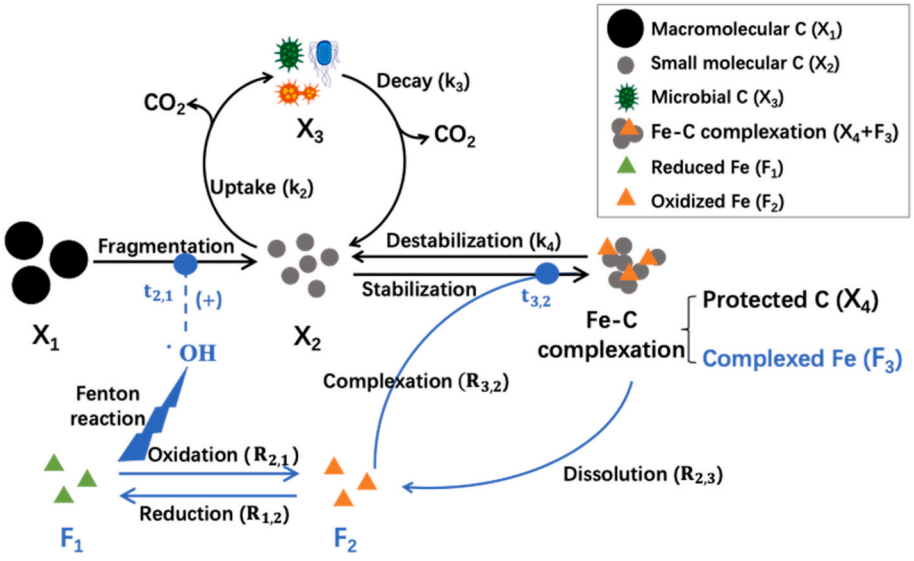

Fig. 1. Conceptual diagram of the microbe-Fe interaction (MiFe) model of lignin decomposition. X_1, X_2, X_3 and X_4 represent macromolecular, small molecular, microbial, and protected carbon pools, respectively. F_1, F_2 and F_3 represent reduced, oxidized, and complexed iron pools, respectively. The solid black line represents carbon fluxes while the solid blue line represents the iron transfer pathway. Detailed descriptions of transfer coefficients can be found in Supplementary Table S2. The blue dashed lines indicate iron-carbon interaction processes. Sign "+" indicates a positive effect. The blue dot means iron-driven transfer. (For interpretation of the references to colour in this figure legend, the reader is referred to the Web version of this article.)

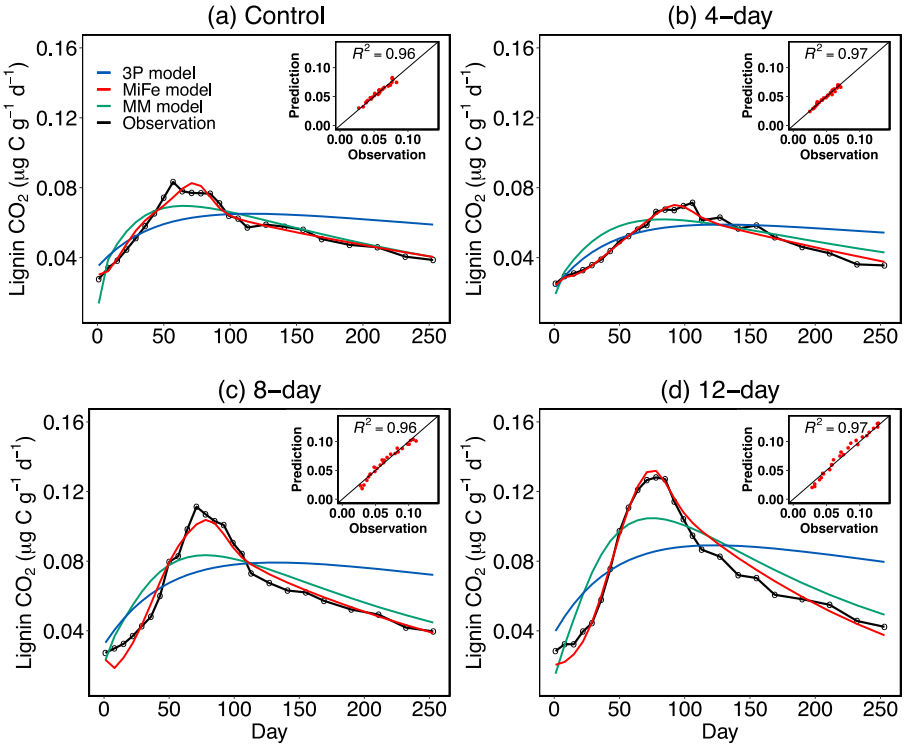

Fig. 2. Observed and simulated CO_2 production rates from lignin decomposition in the Oxisol with four anaerobic pre-treatments. (a) 0-day anaerobic pre-treatment (Control), **(b)** 4-day anaerobic pre-treatment (4-day), **(c)** 8-day anaerobic pre-treatment (8-day), **(d)** 12-day anaerobic pre-treatment (12-day). Three models, i.e., three-pool first-order kinetics model (3P model, blue line), Michaelis Menten model (MM model, green line), and MiFe model with logistic functions (red line), were used to fit observations (black line). Insets are comparison of observations vs. predictions from the MiFe model. (For interpretation of the references to colour in this figure legend, the reader is referred to the Web version of this article.)

a tropical forest (C_3 vegetation) soil rich in reactive Fe minerals, with leaf litter from a C_4 grass and either synthetic $^{13}C_\beta$-labeled or unlabeled lignin. Thus, lignin-C could be discriminated from other C sources (i.e., litter-C and soil-C). Specifically, Huang et al. (2019) incubated soil samples with three types of substrates, including (1) soils alone, (2) soils amended with litter and synthetic lignin (soil + litter + unlabeled lignin), and (3) soils amended with litter and synthetic lignin labeled with 99 atom % ^{13}C at the C_β position of each lignin C substructure (soil + litter + labeled lignin). Samples were pretreated with either 12, 8, 4, or 0 days of anaerobiosis at staggered intervals over the first 12 days of the incubation to generate a gradient of reduced Fe, with more reduced Fe under longer anaerobic pre-treatments. Subsequently, samples after pre-treatments were exposed to an aerobic headspace for 317 days. All soil samples were incubated in glass jars at 23 °C in the dark for total 329 days.

Huang et al. (2019) measured CO_2 production rates and their C isotope ratios ($\delta^{13}C$) from the soil samples every 2 or 4 days in the beginning, weekly after 47 days, and every other week after 189 days. The production of CO_2 derived from $^{13}C_\beta$-labeled lignin was calculated by mixing models described in Huang et al. (2019). Overall, there were 50 sampling times over the whole 329-day incubation period. They found that lignin decomposition increased rapidly after 77 days and peaked at ~4 months. We inferred that microbial community that degraded lignin was built during 77 days at the beginning of incubation, which was difficult to be represented as empirical equations so that the records before 77 days were not included in our models. The lignin decomposition then diverged markedly among the four anaerobic pre-treatments, resulting in significantly more CO_2 production from lignin decomposition in the 12-day anaerobic pre-treatment, followed by the 8-day anaerobic treatment, control, and 4-day anaerobic pre-treatment at the end of the incubation (Huang et al., 2019). To explain the mechanism underlying lignin decomposition, a total of 25 sampling records (from 77 days to 329 days) of the 12-day, 8-day, 4-day anaerobic pre-treatments, and control were used in this study to construct models as described below. In addition, the other experimental information was also applied in this study, such as ^{13}C labeled C mass of the added synthetic lignin at 313.06 μg and total Fe extracted by sodium dithionite at 64 mg in each sample soil.

2.2. Model description

2.2.1. Microbe-Fe interaction (MiFe) model

To mechanistically simulate the observed dynamics of lignin decomposition in the four pre-treatments with different O_2 availability, we developed microbe-Fe interaction (MiFe) models by incorporating the microbe-Fe interactions in lignin decomposition (Fig. 1).

Specifically, the model consists of two main processes: lignin-derived C transformation among different pools and Fe conversion. The conceptualized lignin-C pools include macromolecular lignin C (X_1), small molecular lignin C (X_2), microbial carbon (X_3), and Fe-protected lignin C (X_4). Meanwhile, Fe minerals in soil are divided into reduced Fe(II) (F_1), oxidized Fe(III) that is not associated with lignin C (F_2) and Fe associated with lignin C (F_3). Please note that our modelling analysis was focused only on lignin C decomposition, and we did not include litter decomposition in our model. Also, it is true that lignin is not the only microbial substrate in the process of litter and soil organic C decomposition. However, as this model only considered the process of lignin decomposition, the microbes in the model here were referred to the lignin-degrading organisms, such as white-rot fungi, brown-rot fungi and some bacteria (actinomycetes).

The detailed balance equations for each pool can be found in Table S1 of supplementary materials. The dynamics of lignin C pools and Fe pools can be described by the following two matrix equations:

$$\frac{dX}{dt} = A_1KX(t) + A_2TX(t) \quad (1)$$

$$\frac{dF}{dt} = RF(t) \quad (2)$$

where the C decomposition $\left(\frac{dX}{dt}\right)$ is controlled by both the microbe-dominated process $(A_1KX(t))$ and iron-coupled transformation ($A_2KX(t)$). In the beginning, the pool size of each pool is given by a proportion

($X_{1,0}$, $X_{2,0}$, $X_{3,0}$ and $X_{4,0}$) of total lignin ^{13}C-labeled C amount. For example, the initial proportion of macromolecular lignin C (X_1) is $X_{1,0}$. In Eq. (1), K is a matrix that expresses the C decomposition rates of different C pools driven by microbial activity. Matrix A_1 represents the transfer coefficients at which decomposed C is transferred from one pool to another. Similarly, while matrix T shows the transfer rates of Fe pools, A_2 indicates the transfer fractions among different Fe pools.

Specifically, A_1, A_2, K, and T were written as:

$$A_1 = \begin{pmatrix} 0 & 0 & 0 & 0 \\ 0 & -1 & a_{2,3} & 1 \\ 0 & a_{3,2} & -1 & 0 \\ 0 & 0 & 0 & -1 \end{pmatrix} \quad (3)$$

$$K = \begin{pmatrix} 0 & 0 & 0 & 0 \\ 0 & k_2 & 0 & 0 \\ 0 & 0 & k_3 & 0 \\ 0 & 0 & 0 & k_4 \end{pmatrix} \quad (4)$$

$$A_2 = \begin{pmatrix} -1 & 0 & 0 & 0 \\ 1 & -1 & 0 & 0 \\ 0 & 0 & 0 & 0 \\ 0 & 1 & 0 & 0 \end{pmatrix} \quad (5)$$

$$T = \begin{pmatrix} t_{2,1}*R_{2,1}*F_1 & 0 & 0 & 0 \\ 0 & t_{4,2}*R_{3,2}*F_2 & 0 & 0 \\ 0 & 0 & 0 & 0 \\ 0 & 0 & 0 & 0 \end{pmatrix} \quad (6)$$

where k_i represents the decay rate of ith C pool, but with k_4 referring to the destabilized rate of X_4. Each item $a_{i,j}$ is the C transfer coefficient, representing the fraction of C being transferred from the donor pool j to the recipient pool i. Among these transfer coefficients, $a_{3,2}$ indicates the fraction of the depolymerized small molecular lignin C (i.e., X_2) used in microbial metabolism to build microbial biomass (i.e., X_3). Therefore, $a_{3,2}$ is the conversion efficiency for lignin C, regarded as the microbial carbon use efficiency (CUE) of lignin. In matrix T, the transfer rates of lignin C pools (from C pool i to j) can be expressed as $t_{j,i}*R_{j,i}*F_i$, where $t_{j,i}$ represents the coupled coefficients between C transfer and Fe conversion. $R_{j,i}$ indicates the conversion rate of Fe from the pool i to j and F_i is different Fe pools.

R in Eq. (2) indicates the transfer rates between Fe pools, which can be described as follows:

$$R = \begin{pmatrix} -R_{2,1} & R_{1,2} & 0 \\ R_{2,1} & -(R_{1,2} + R_{3,2}) & R_{2,3} \\ 0 & R_{3,2} & -R_{2,3} \end{pmatrix} \quad (7)$$

Each item $R_{i,j}$ in matrix R in Eq. (7) indicates the transfer rate of Fe from the pool j to i. According to the empirical studies, we assumed that the breakdown of macromolecular C into small molecular C is determined by Fe(II) concentration and the transfer rate from Fe(II) to Fe(III) ($R_{2,1}$) by $t_{2,1}$ (Eq. (6)). The concentration of Fe(III) controls the transfer of small molecular C to protected C by $t_{4,2}$ (Eq. (6)).

Different from traditional first-order kinetic scheme in biogeochemical models, we adopted the following Logistic Equations (Eqs. (8) and (9)) to simulate the nonlinear growth of microorganisms (McKendrick and Pai, 1911). Logistic Equation is an optimal mathematical model to describe the law of population growth under the condition of limited resources. The initial stage of growth is approximately exponential. Then, as saturation begins, the growth slows to linear and at maturity, growth stops. Eq. (8) described the uptake rate of small molecular lignin C in microbial synthesis, Eq. (9) expressed the mortality rate of microbes.

$$k_2 = \frac{\theta_1}{1 + e^{-\theta_2(t-\theta_3)}} \quad (8)$$

$$k_3 = \frac{\theta_4}{1 + e^{-\theta_5(t-\theta_6)}} \quad (9)$$

where k_2 and k_3 refers to the time-dependent (t) microbial uptake function and microbial decay function, respectively. θ_1, θ_2 and θ_3 indicate the maximum rate, growth rate and lag phase in uptake function, respectively, whereas θ_4, θ_5 and θ_6 constitute the maximum rate, decay rate and lag phase, respectively, in the decay function.

There are a total of 20 parameters in the MiFe model. We used Bayesian Markov Chain Monte Carlo (MCMC) technique (as described below) with the experimental data of lignin-derived CO_2 production after 77-day incubation published in Huang et al. (2019) to estimate all the model parameters.

2.2.2. Microbe-Fe interaction model with Michaelis-Menten kinetics (MM model)

Moreover, in a separate model, we also applied Michaelis-Menten kinetics (microbe-Fe interaction models with Michaelis-Menten kinetics, MM model) instead of using logistic equations to explore the most suitable microbial growth patterns. The Michaelis-Menten kinetics in the microbe-dominated processes is assumed to be the function of substrate availability and enzymatic activity (Schimel and Weintraub, 2003; Wieder et al., 2013). The Michaelis–Menten equation has the same form as the Monod equation (Monod, 1949), but the difference between them is that the Monod equation is based on empirical while the Michaelis–Menten equation is based on theoretical considerations. It can also be used to describe a relationship between microbial specific growth rate and the presence of a single limiting substrate.:

$$k_2 = V_{max1}\left(\frac{X_2}{X_2 + K_{s1}}\right) \quad (10)$$

$$k_3 = V_{max2}\left(\frac{X_3}{X_3 + K_{s2}}\right) \quad (11)$$

In this formulation, the decomposition rate will be limited by substrate availability (small molecular C, X_2 or microbial C, X_3). Each of the Michaelis-Menten equation is based on two key parameters: V_{maxi}, the maximum growth rate of this microorganism and K_{si}, the substrate half-saturation constant. They will differ between microorganism species and will also depend on the ambient environmental conditions, e.g., temperature, pH of the solution, and the composition of the culture medium (Monod, 1949). Except for equations (10) and (11), the structure and equations of MM model are consistent with those of MiFe model. A total of 18 parameters in the MM model were estimated by MCMC technique as well.

2.2.3. Non-Fe model

To examine the relative importance of the Fe-mediated stabilization in the dynamics of lignin CO_2 production, we established a non-Fe model based on the MiFe model. The only difference between the non-Fe model and the MiFe model is that the transfer coefficients represented by T do not couple with Fe pools (Eq. (12)) in the non-Fe model to remove microbe-Fe interactions on lignin decomposition.

$$T = \begin{pmatrix} t_{2,1} & 0 & 0 & 0 \\ 0 & t_{4,2} & 0 & 0 \\ 0 & 0 & 0 & 0 \\ 0 & 0 & 0 & 0 \end{pmatrix} \quad (12)$$

A total of 20 parameters in the non-Fe model were estimated by MCMC technique. We only tested the 12-day anaerobic pre-treatment for the non-Fe model to illustrate the role of Fe in SOC stabilization.

2.2.4. 3-Pool transfer model

In most of the terrestrial C cycle models, the soil organic matter (SOM) decomposition module is represented by multiple C pools and

uses a first-order kinetic scheme (Parton et al., 1993; Bondeau et al., 2007; Adair et al., 2008; Clark et al., 2011; Koven et al., 2013). In this study, we firstly applied a first-order 3-pool (3P) transfer model, which is the traditional structure derived from the CENTURY and TECO models (Parton et al., 1993; Luo et al., 2003), to simulate the lignin C transfer (Supplementary Fig. S1). The 3P model consists of three C pools, theoretically separating the lignin C into active, slow and passive components with their respective decay rate. The dynamics of lignin C is realized through transfers among these three pools, which can be formulated to a matrix equation as follows:

$$\frac{dP}{dt} = AKP(t) \tag{13}$$

where P(t) is a 3 × 1 vector indicating lignin C pool sizes. Matrix A represents the C transfer coefficient and K is a 3 × 3 matrix with each diagonal element representing the turnover rate of each C pool as:

$$A = \begin{pmatrix} -1 & f_{1,2} & f_{3,1} \\ f_{2,1} & -1 & 0 \\ f_{3,1} & f_{3,2} & -1 \end{pmatrix} \tag{14}$$

$$K = \begin{pmatrix} k_1 & 0 & 0 \\ 0 & k_2 & 0 \\ 0 & 0 & k_3 \end{pmatrix} \tag{15}$$

where each item $f_{i,j}$ in Eq. (14) is C transfer coefficient, representing the fraction of C from the pool j to i. k_i in Eq. (15) refers to decay rate of ith C pool. The above structure and the matrix equations have been widely used and verified in biogeochemical research (Xu et al., 2006, 2016; Liang et al., 2015). We applied the 3P model accompanied by data assimilation with the incubation data to examine the first-order decay hypothesis.

2.3. Data assimilation

Probabilistic inversion approach (Eq. (16)) based on Bayes' theorem was used to estimate parameters in this study (Xu et al., 2006; Tao et al., 2020):

$$P(\theta|Z) \propto P(Z|\theta)P(\theta) \tag{16}$$

where $P(\theta|Z)$ is the posterior probability density function of model parameters θ, which can be obtained from the likelihood function $P(Z|\theta)$ and prior probability density function $P(\theta)$. $P(\theta)$ represents the assumption range of parameters θ based on empirical knowledge. $P(Z|\theta)$ is the conditional probability density of parameter θ under observation Z, which is defined as the likelihood function. For a given observation Z and a specific model, $P(Z|\theta)$ can be calculated with the following equation with the assumption that model prediction errors are independent and follow a multivariate Gaussian distribution with a zero mean (Liang et al., 2015):

$$P(Z|\theta) \propto \exp\left\{ -\sum_{i=1}^{k} \frac{[z_i(t) - x_i(t)]}{2\sigma_i^2(t)} \right\} \tag{17}$$

where z_i and x_i indicate modeled and observed values, respectively. σ_i is the standard deviation of the observations and k is the number of observations. In this study, observations refer to the incubation data from Huang et al. (2019).

To generate the posterior distributions of parameters, Metropolis-Hastings (M-H) algorithm was used to do the probabilistic inversion (Haario et al., 2001), which is a Markov Chain Monte Carlo (MCMC) technique (Metropolis et al., 1953; Hastings, 1970). The new parameter values were proposed uniformly within their proposed prior range (Hararuk et al., 2014):

$$\theta^{new} = \theta^{old} + \frac{d(\theta_{max} - \theta_{min})}{D} \tag{18}$$

where θ^{new} is the new proposed parameter value and θ^{old} is the accepted parameter value in the last step. θ_{min} and θ_{max} represent the upper and lower limits of proposed prior range, respectively. d is a uniformly distributed random variable between −0.5 and 0.5 to help find an appropriate new parameter value randomly in the moving step. D is a coefficient to control the proposing step size, which could vary with models.

Uniform Metropolis criterion was used to determine whether the new parameter values would be accepted (Xu et al., 2006). The M-H algorithm was formally run with 5 replicates and 200,000 times for each replicate for statistical analysis of the parameters. Due to the randomness of each replicate, only the last half of the accepted parameter values were used to generate posterior distribution. And we took the averages of the last hundred accepted parameter values as the optimal parameter values. Overall, the targeted parameters in the MiFe model were effectively constrained by data assimilation (Supplementary Fig. S5), especially for the initial proportion of lignin C pools and Fe(II) and Fe(III), transformation coefficient and coefficients of microbial uptake and decay functions. However, the parameters for transfer rates were not well constrained, which might be due to the weak signals from incubation data. In fact, only a very small proportion (less than 1%) of the measured CO_2 was produced from the Fe-protected lignin C so that the current observation could not provide enough information to constrain those parameters.

The convergence of the simulated Markov Chains was further tested by the Gelman-Rubin (G-R) diagnostic method to ensure that the within-run variation was roughly equal to the between-run variation (Gelman and Rubin, 1992). If the number of parallel M-H runs is M and the number of accepted iterations is N, the between and within-run variations of *i*th parameter can be calculated using the following equation:

$$W_i = \frac{1}{M} \sum_{m=1}^{M} \sigma_m^2 \tag{19}$$

$$B_i = \frac{N}{M-1} \sum_{m=1}^{M} (\bar{p}^{\cdot,m} - \bar{p}^{\cdot\cdot})^2 \tag{20}$$

where $\bar{p}^{\cdot,m}$ and σ_m represent the mean and standard deviation of the specific parameter in the *m*th replicate, and $\bar{p}^{\cdot\cdot}$ is the mean of the specific parameter over the M replicates. G-R statistic of specific parameter is defined as:

$$GR_i = \sqrt{\frac{W_i(N-1)/N + B_i/N}{W_i}} \tag{21}$$

In this study, the GRs of all parameters of the four pre-treatments approached 1, which indicates the Markov chain reached convergence.

2.4. Statistical analysis

Common statistical analysis methods were used to evaluate the fitness of models, including the coefficient of determination R^2 (comparison between the observed and simulated data), Root Mean Square Error (RMSE), Mean Absolute Percent Error (MAPE) and Akaike information criterion (AIC). For total n data points, the formulas of R^2, RMSE, MAPE and AIC (Akaike, 1974; Burnham and Anderson, 2004) are as follows:

$$R^2 = \left[1 - \frac{\sum_{i=0}^{n} (P_i - Obs_i)^2}{\sum_{i=0}^{n} (Obs_i - \overline{Obs})^2} \right] \times 100\% \tag{22}$$

$$RMSE = \frac{1}{n}\sum_{i=0}^{n}(P_i - Obs_i)^2 \quad (23)$$

$$MAPE = \frac{1}{n}\sum_{i=0}^{n}\left|\frac{(P_i - Obs_i)}{Obs_i}\right| \times 100\% \quad (24)$$

$$AIC = n\ ln\left[\frac{\sum_{i=0}^{n}(P_i - Obs_i)^2}{n}\right] + 2b \quad (25)$$

where P_i is the prediction of the fitted model and Obs_i is the corresponding observation and $\overline{Obs}$ is the mean of all observed respiration rates. b in Eq. (25) refers to the number of estimated model parameters. In this study, we used R^2 as the main basis to evaluate model performance. The R^2 value quantifies how well the model fits observations. The closer the R^2 value approaches 1, the better the model fits the observation. Both RMSE and MAPE were reported to provide additional evaluations comparing the differences between the model simulations and observations. The RMSE is a measure of accuracy that compares simulated errors of different models for a particular dataset (Hyndman and Koehler, 2006). The RMSE value, always a positive value, decreases as the error approaches zero. Different from RMSE, MAPE also considers the magnitude of observed data and thus offers intuitive interpretation in terms of relative error. Considering both of the fitting goodness and the model simplicity, we used AIC value to comprehensively evaluate the performance of each model. The model with a smaller AIC value is more parsimonious (Liang et al., 2015).

We presented the optimal model results from the 5 replicated simulations for each pre-treatment. The average of the 5 optimal parameter values was accepted as the final estimated parameter value. We conducted one-way analysis of variance (ANOVA), with Duncan tests to compare differences of parameters among pre-treatments at 95% confidence level (P-value < 0.05). All of the above statistics were performed with R (version 3.6.2) software.

3. Results

3.1. Mechanisms underlying lignin C decomposition

This study identified the microbe-Fe interactions as represented in the MiFe model as the most parsimonious mechanism that can adequately reproduce the dynamic changes of CO_2 production from lignin decomposition in all four anaerobic pre-treatments (Fig. 2). In the incubation experiment, soil was pre-treated with 12, 8, 4, or 0 days of anaerobic conditions during the first 12 days and was in an aerobic incubation for subsequent 317 days. These pre-treatments are hereafter termed 12-day, 8-day, 4-day, and control. The MiFe model fit the observed data well with coefficients of determination (R^2) between 0.96 and 0.97 (Table 1 and Fig. 2). The Root Mean Square Error (RMSE) values were very close to 0, and Mean Absolute Percent Error (MAPE) values were lower than 9% across all the pre-treatments (Table 1). In addition, the MiFe model had the lowest AIC value among the models that we evaluated. From the dynamic patterns of CO_2 production, we inferred that there should be accumulation of relatively accessible lignin C for microbes to induce an exponential increase of lignin decomposition. We incorporated the plausible mechanism in the MiFe model by assuming that such accumulated lignin C was derived from the breakdown of macromolecular lignin linked to Fe oxidation that produced reactive oxygen species such as hydroxyl radical accumulated in the soil. Thus, this accumulation and delayed consumption of small molecular C by microorganisms led to insufficiency of the first-order kinetic 3-pool (3P) model in describing the observed dynamics of lignin C decomposition, especially for different peak heights among the four pre-treatments (Fig. 2). The R^2 values for fitting the observed data with the 3P model ranged from 0.36 to 0.60 for the four pre-treatments (Table 1).

The MiFe model with time-dependent logistic functions was much better than Michaelis-Menten functions (i.e., the MM model) to represent the delay process before the exponential decomposition of small molecular lignin C occurred, which was followed by substrate limitation. In comparison, the microbe-substrate reactions as represented in the MM model did not fit the observations well (Table 1). The MM model simulated relatively smooth curves and did not capture the observed patterns of rapid increases and decreases of CO_2 production from lignin decomposition, especially for the 8-day and 12-day anaerobic pre-treatments (Fig. 2).

Moreover, we represented the mechanism for lignin stabilization in the MiFe model by assuming that the small molecular lignin C from both breakdown of macromolecular lignin via the Fenton reaction and that necromass of dead microbes and small molecular lignin C were stabilized through association with Fe minerals to form the Fe-protected C (Hall and Silver, 2013; Chen et al., 2020). We also developed a non-Fe model to examine the relative importance of the Fe-mediated stabilization in the dynamics of CO_2 production from lignin decomposition. The non-Fe model significantly overestimated the respiration rates during the late incubation period although it still captured the CO_2 production peak (Supplementary Fig. S2). The non-Fe model also simulated higher CO_2 production from lignin decomposition than the MiFe model (Supplementary Fig. S2). The remaining lignin C during the later stage of simulation was more preserved in the form of macromolecular C (44.0%) in the non-Fe model than in the MiFe model (41.1%) (Supplementary Fig. S3). The results further indicated that Fe played a crucial role in lignin decomposition and SOC persistence.

3.2. Key processes determining lignin C decomposition

Differences in CO_2 production among the four pre-treatments could be primarily explained by variations in initial C and Fe pool sizes of the simulations, C transfer rates, and microbial uptake rates (Fig. 3 and Supplementary Table S2). Generally, the duration of the initial anaerobic pre-treatment controlled Fe reduction and thus affected the subsequent lignin decomposition process through altering the abundance of reduced Fe and microbial activities. The initial value of Fe(II) ($\mathbf{F_{1,0}}$) increased with the anaerobic duration of the pre-treatments (Fig. 3a),

Table 1
Measures of data-model fittings. Determination coefficient (R^2) values, Root Mean Square Error (RMSE) and Mean Absolute Percent Error (MAPE) were used to measure the goodness-of-fit of the microbe-Fe interaction (MiFe) model, 3-pool transfer (3P) model and Michaelis-Menten kinetics (MM) model in simulating lignin CO_2 production rates under 0-day (Control), 4-day, 8-day, and 12-day anaerobic pre-treatments. Akaike information criterion (AIC) was used to evaluate the simplicity of models.

Treatments	MiFe model				3P model				MM model			
	R^2	RMSE (μg C g^{-1} d^{-1})	MAPE (%)	AIC	R^2	RMSE (μg C g^{-1} d^{-1})	MAPE (%)	AIC	R^2	RMSE (μg C g^{-1} d^{-1})	MAPE (%)	AIC
Control	0.958	0.003	4.30	−248.6	0.393	0.012	19.0	−202.0	0.804	0.007	10.5	−214.2
4-day	0.974	0.002	3.28	−265.6	0.603	0.009	14.9	−217.2	0.704	0.008	15.1	−208.5
8-day	0.962	0.005	7.57	−225.2	0.363	0.020	31.0	−174.7	0.730	0.013	18.7	−180.2
12-day	0.972	0.005	8.11	−220.7	0.365	0.026	35.3	−162.9	0.785	0.015	20.5	−174.0

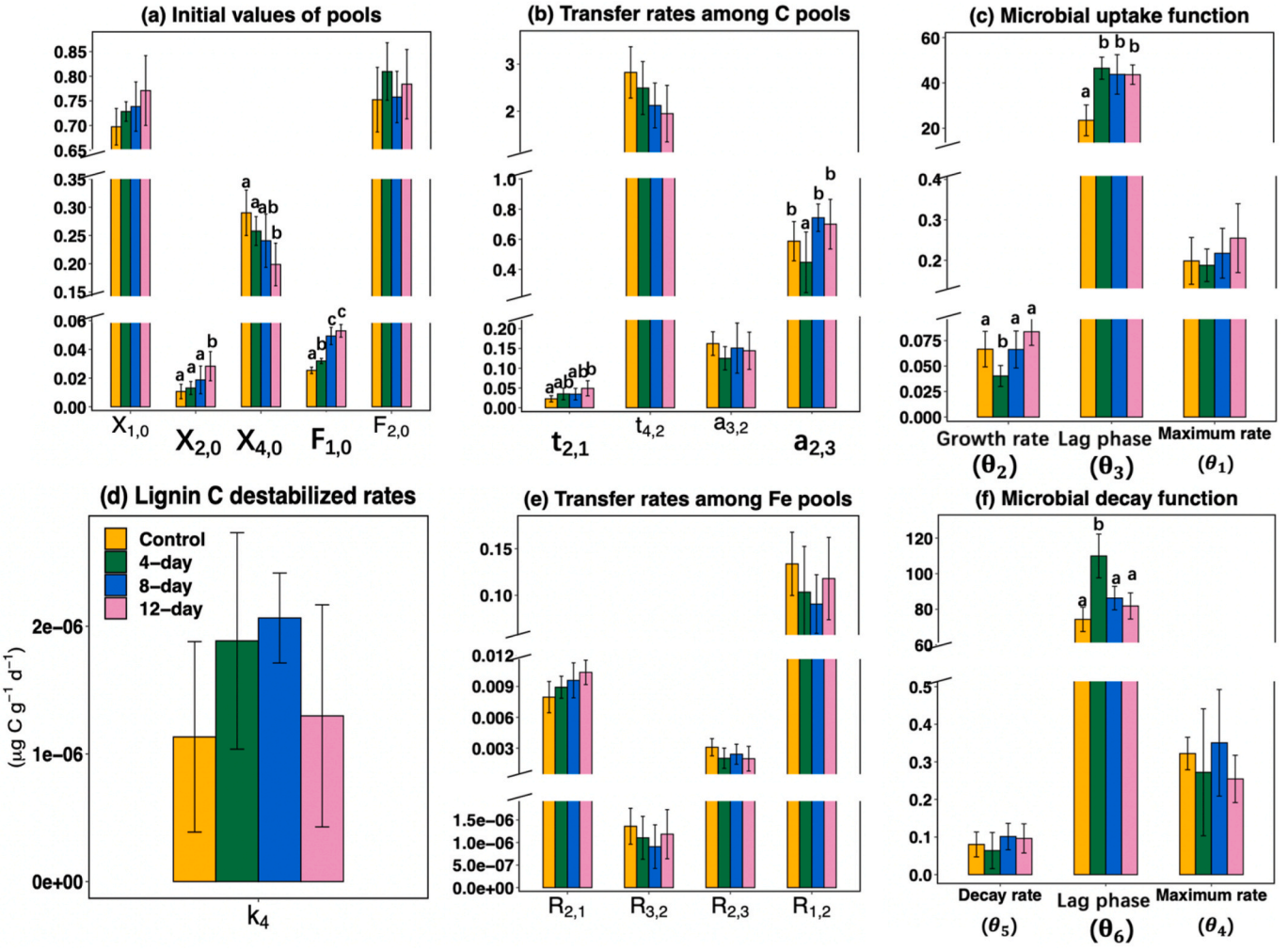

Fig. 3. Comparison of parameter values of the MiFe model among the four pre-treatments. Parameters are **(a)** the proportions of initial C and Fe values, **(b)** transfer rates among C pools, **(c)** microbial uptake function, **(d)** lignin C destabilized rates, **(e)** transfer rates among Fe pools, and **(f)** microbial decay function. Labels in bold on x-axis and different size letters indicate significant differences between the pre-treatments at P-value < 0.05. Detailed descriptions of parameters can be found in Supplementary Table S2.

consistent with the experimental observations in Huang et al. (2019). The greater initial values of small molecular C ($\mathbf{X_{2,0}}$) in the longer anaerobic pre-treatments likely resulted from stronger lignin depolymerization induced by the Fenton reaction than the shorter anaerobic pre-treatments (Wood, 1994; Hammel et al., 2002). Consequently, the ability of microbes to use C when C was abundant, which was represented by logistic growth rate (θ_2) in the MiFe model, increased from the 4-day to 12-day anaerobic pre-treatments but not in the control (Fig. 3c). The delay effect of microbial uptake function as described by the half-life time ($\boldsymbol{\theta_3}$) was higher in the 4-, 8- and 12-day anaerobic pre-treatments than in the control (Fig. 3c). On the other hand, the lag phase of microbial decay function ($\boldsymbol{\theta_6}$) was longer in the 4-, 8- and 12-day anaerobic pre-treatments (Fig. 3f).

The non-Fe model simulation showed that when there was no Fe effect on lignin decomposition, similar peak height in the 12-day pre-treatment was simulated by a lower lag phase ($\boldsymbol{\theta_3}$) in microbial uptake function (Supplementary Fig. S4b). Relative to the MiFe model, the maximum decay rate ($\boldsymbol{\theta_4}$) in microbial decay function was higher in the non-Fe model, which was expected to decline lignin decomposition to a greater extent after the peak. However, such a decline in the non-Fe model was not enough to compensate for the lack of Fe stabilization effect (Supplementary Fig. S4b), which resulted in higher lignin decomposition after the peak and eventually failed to fit the observations (Supplementary Fig. S2). Our results further suggested that discounting the microbe-Fe interactions made it harder to explain the observed dynamic patterns of CO_2 production from lignin decomposition.

3.3. Fates of lignin carbon

Our analysis with the MiFe model revealed dynamic patterns of four C pools, i.e., macromolecular lignin C, small molecular lignin C, microbial biomass C, and protected C via Fe association, as depicted in Fig. 1. During the period of incubation we analyzed (77–329 days), the amount of macromolecular C declined whereas the protected C increased. The small molecular C was initially high but depleted to almost zero toward the end of the incubation. In contrast, the microbial biomass C of lignin-degrading organisms was initially low, peaked at 40–70 days after the pseudo-equilibrium of microbial dynamics, and finally declined to almost zero at the end of the incubation.

The four pre-treatments did not significantly change the overall patterns of the four C pools but resulted in different rates of transformation. The 8- and 12-day anaerobic pre-treatments stimulated the transformation rate of the macromolecular lignin to small molecular lignin C to a greater extent than the 0- and 4-day pre-treatments (Fig. 4a). Correspondingly, the small molecular lignin C initially was much higher and microbial processes were more active in the 8- and 12-day than 0- and 4-day pre-treatments (Fig. 4b, d). Given the higher rates

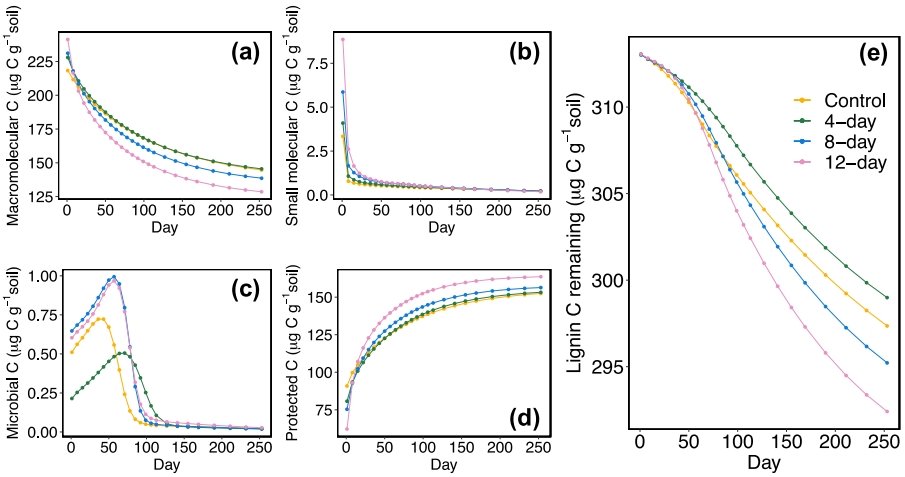

Fig. 4. Lignin C dynamics in different pools under four anaerobic pre-treatments.

of transformation, the protected C was higher (Fig. 4c) but the total C remaining was lower (Fig. 4e) in the 8- and 12-day than 0- and 4-day pre-treatments.

During the period of incubation, lignin C was depolymerized, partly being respired as CO_2 and partly being stabilized through Fe–C association. The 8- and 12-day anaerobic pre-treatments had more respiration than the 0- and 4-day pre-treatments (Fig. 5). At the end of the incubation, the remaining lignin C was mainly in the form of macromolecular C and protected C whereas the small molecular C and microbial C were almost exhausted. Macromolecular C was significantly less depolymerized and this led to higher portions remaining in the 0- (46.2%) and 4-day (46.5%) than the 8-day (44.3%) and 12-day pre-treatments (41.1%). A greater portion of the lignin C was protected by Fe as the duration of anaerobic pre-treatments increased (Fig. 5). The 12-day anaerobic pre-treatment had 52.3% protected C while the control only accrued 48.7% (Fig. 5).

Overall, the protected C in the 12-day anaerobic pre-treatment increased by about 100 μg C g^{-1} soil relative to the initial value (Fig. 4d). We further investigated the contributions of fragmented lignin C versus microbial-derived C to the mineral-associated lignin C pool. Conceptually, the Fe-protected lignin C was derived from small molecular C and microbial products or necromass, as also described in the MiFe model. During the period of incubation we analyzed, microbial-derived C was less than 3 μg C g^{-1} soil, accounting for a small proportion of the Fe-protected C (<3%). Most of the Fe-protected C was derived from the small molecular lignin C rather than microbial-derived C.

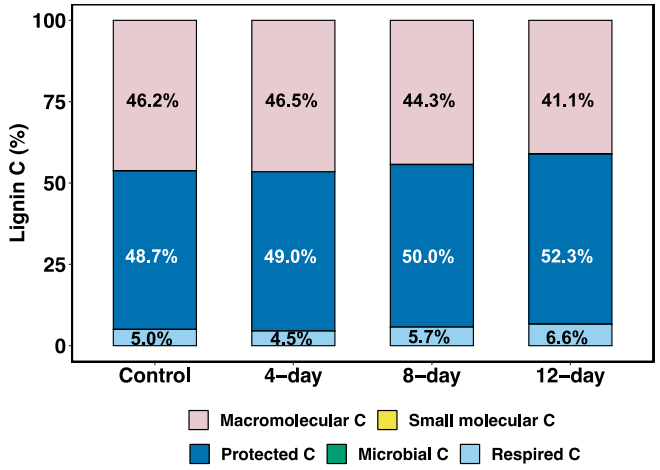

Fig. 5. Fates of lignin C at the end of this analysis in the four anaerobic pre-treatments. The amount of both small molecular C and microbial C is too small in the later stage of incubation to be displayed in the figure.

4. Discussion

Building upon the representative dataset from Huang et al. (2019), our data-model integration proposed a new lignin decomposition framework, which revealed the underlying mechanisms controlling the temporal dynamics of lignin decomposition and lignin fate in soils. Such dynamics are not easily measurable in laboratory studies. Different from the study by Huang et al. (2019), our modeling results clearly demonstrated the progressive patterns of how lignin C was metabolized by microbes and stabilized by minerals. We also revealed the critical processes/parameters that controlled lignin decomposition, and mechanistically explained the observed lignin decomposition as a function of redox-sensitive biogeochemical reactions. Finally, this study further analyzed lignin fate in soil by estimating microbial lignin-C use efficiency and quantifying dynamic microbe-Fe interactions, neither of which are easily measured in laboratory experiments. In general, our study offers not only a new modeling framework to study lignin decomposition via microbe-Fe interactions but also quantitative evidence on the importance of lignin contribution to SOC persistence.

4.1. Role of microbe-iron interactions in lignin decomposition

Our results indicated that microbe-Fe interactions significantly regulated lignin C decomposition and stabilization. Based on experimental data from Huang et al. (2019) and the mechanistic model developed in this study, we inferred that the reduced Fe in the anaerobic pre-treatments activated the Fenton reaction to break down macromolecular lignin C into small molecular C. The small molecular lignin C was consumed by microorganisms, including both bacteria and lignin-degrading fungi (Kirk and Farrell, 1987), to produce CO_2 (Fig. 1). Accumulation of the small molecular C stimulated colonization of microorganisms, which appeared to last about 10 weeks (observed from data) before microbes exponentially grew in accompany with a burst of respiratory C release. This might be due to the fact that the small molecular lignin C was very likely metabolized by a large group of microbial community (not only limited to fungi) after macromolecular lignin C was depolymerized by Fenton reaction. In addition, microbial-derived C accounted for a very minor fraction of the increased protected C (<3%) during the period of this analysis. The stabilized C, mainly through sorption and/or co-precipitation to Fe oxides, was mainly derived from small molecular lignin C.

4.2. Contributions of plant-derived vs. microbial-derived C to mineral associated organic matter (MAOM)

Mineral (e.g., Fe) protective effects have been widely recognized as an important mechanism of SOC persistence (Lalonde et al., 2012; Zhao et al., 2016; Coward et al., 2017; Fang et al., 2019). However, the contributions of plant-derived vs. microbial-derived C to mineral associated organic matter (MAOM) remain controversial (Cotrufo et al., 2013; Huang et al., 2019). The Microbial Efficiency-Matrix Stabilization (MEMS) hypothesis proposes that microbial-derived C preferentially accumulates in MAOM by promoting aggregation and through strong chemical bonding to the minerals (Cotrufo et al., 2013, 2015). Here, our data-model integration provides an alternative mechanism whereby plant-derived materials can provide a significant C source to MAOM while it is acknowledged that microbial products are also an important constituent of MAOM (Miltner et al., 2011; Kallenbach et al., 2016). Although we did not investigate the total necromass contributions from other litter C components, our modeling results showed that microbial-derived lignin C (<3 μg C g^{-1} soil) contributed only a small fraction to the large amount (~100 μg C g^{-1} soil) of Fe-associated C, at least during the period of our analysis. The small contribution of microbial-derived lignin C to MAOM, as a result of the low microbial C-use efficiency of lignin C (Martin et al., 1980; Bahri et al., 2008), was consistent with the MEMS hypothesis (Cotrufo et al., 2013). However, small molecular lignin C produced by Fenton reaction or other abiotic processes may contribute more than microbial bioproducts or necromass to the mineral-protected C. The direct interaction between small molecular lignin derivatives and Fe appeared to dominate. Therefore, contributions of plant-derived C to MAOM may be underestimated in some soils, especially those with large inputs of lignin C and high concentrations of Fe minerals.

The traditional concepts consider lignin as a main component of SOC due to its inherent chemical recalcitrance (Lützow et al., 2006; Adani et al., 2007; Kleber, 2010). Recent experimental research demonstrated that instead of molecular structures of litter and lignin, environmental and biological factors predominated SOC stability (Schmidt et al., 2011; Woolf and Lehmann, 2019), implying less contributions by lignin to SOC persistence (Schmidt et al., 2011). However, both the data from the soil incubation (Huang et al., 2019) and our analysis suggested that nearly half of lignin C would be preserved as Fe-associated C partly because of direct interactions of lignin C with minerals even though microbial C-use efficiency of lignin was low (about 15% in this study). Although we did not further detect whether lignin was physically protected or chemically bound within Fe-associated C, it is certain that the small molecular lignin directly combined with Fe to form protected C (Riedel et al., 2013; Hall et al., 2016; Angst et al., 2017; Córdova et al., 2018). Incorporation of Fe effects on lignin stabilization would be helpful to mechanistically understand the persistence of lignin and SOC.

4.3. Decomposition models

In this study, we used the data-driven approach to discover that logistic equations can best describe a nonlinear pattern of respired CO_2 from lignin decomposition in soil as observed by Huang et al. (2019). Traditionally, models with the first-order kinetics and/or Michaelis-Menten equations have been used to describe decomposition of litter and SOM. The first-order kinetics models usually describe exponential delay patterns, which have been observed from almost all litter and SOM decomposition studies (Zhang et al., 2008; Schadel et al., 2014; Xu et al., 2016; Cai et al., 2018; Luo and Smith, 2022). Michaelis-Menten equations, however, have been recently incorporated into dozens of new microbial models (Aneesh Chandel et al. *In prep.*) to express the notion that microbial catalysis is presumably a rate-limiting step in litter and SOM decomposition (Allison et al., 2010). The models with Michaelis-Menten equations usually generate nonlinear patterns of CO_2 release from organic matter decomposition (Wang et al., 2014). The pattern observed by Huang et al. (2019) was the only nonlinear one we have found so far and, thus, could offer direct empirical evidence to support Michaelis-Menten kinetics of organic matter decomposition. We did first use a Michaelis-Menten model to fit the data. As shown in Fig. 2, the Michaelis-Menten model cannot describe the observed pattern well. That forced us to search for other models. After a few tries, we found that the MiFe model with logistic equations fit data best (Fig. 2). A possible explanation for the logistic equations to fit the observed pattern well is related to the time course of establishment and growth of microbial populations and community.

While lignin is a large part of litter, Huang et al. (2019) found that CO_2 production from lignin accounts for only a small fraction (about 0.1%) of the total respired CO_2 by litter due to its low degradation rate. The time courses of CO_2 production from litter decomposition were slightly modified by lignin degradation but still could be approximated by a classical 2- or 3-pool model (data not shown here). Nevertheless, our MiFe model could capture the dynamics of lignin decomposition, one key component of litter, with the underlying mechanisms well explained. Our study represents one crucial step towards understanding mechanisms beyond classical multi-pool models. Decomposition processes of different components of litter and soil organic C, such as labile litter C (e.g., starch and semi-cellulose), other structural litter C (e.g., cellulose vs. lignin), particulate organic matter (POM), and MAOM, were regulated by various environmental factors. For example, this study especially illustrates lignin is particularly susceptible to regulation of microbe-Fe interactions while the total litter may be less so. Lignin decomposition that was regulated by Fe redox cycling may have little influence on the overall litter decomposition, while lignin-derived C associated with Fe may persist in soil over a long timescale. The lack of mechanistic understanding of decomposition processes of the individual components of litter and soil will bring great uncertainty about the whole prediction of land C persistence in the future.

4.4. Implications for decomposition and persistence of SOC

Our results may shed light on lignin decomposition through the microbe-Fe interactions in field. Frequent O_2 fluctuations can potentially alter soil Fe composition by promoting Fe reduction and increasing or decreasing Fe crystallinity (Winkler et al., 2018), which could conceivably lead to decomposition or stabilization of lignin C (Chen et al., 2018; Huang et al., 2021). It is very common that temporary O_2 limitation exists in soil microsites to induce Fe redox cycling (Hall et al., 2015; Keiluweit et al., 2017) and consequently to influence lignin decomposition and the persistence of SOC. However, the mineral phase changes induced by temporary redox fluctuations have not been accounted in modeling to determine lignin fate. The explicit MiFe model is a plausible and testable model to simulate the persistence of lignin in soils under redox fluctuations as validated by the experimental data. In addition, our model can be applied to quantify the critical roles of microbes and Fe in lignin decomposition and SOC persistence, as well as the relative contributions of microbial-derived vs. plant-derived lignin C to MAOM.

In the future, we need more coordinated empirical-modeling studies (Luo et al., 2011) to examine how different microbial communities affect lignin C stabilization beyond the substrate availability. Indeed, observation of respired CO_2 is limited for modeling. These models require a more comprehensive model evaluation to validate the decomposition processes, in which both fluxes and state variables are compared to observations. In addition, more empirical evidence from different ecosystems and at different timescales is needed, in tandem with modeling analysis, to quantify the relative contributions of microorganisms and minerals, including Fe, to the persistence of SOC in redox-dynamic soils.

Declaration of competing interest

The authors declare that they have no known competing financial interests or personal relationships that could have appeared to influence the work reported in this paper.

Data availability

Data will be made available on request.

Acknowledgement

This work is supported by the National Key Research and Development Program of China (2020YFA0607900, 2020YFA0608003) and the National Natural Science Foundation of China (42125503, 42075137). The authors greatly appreciate the constructive comments by Dr. Steven Hall. Contributions from YL to this work was financially supported by US National Science Foundation (DEB 1655499, DEB 2017884), US Department of Energy (DE-SC0020227), and the subcontracts 4000158404 and 4000161830 from Oak Ridge National Laboratory (ORNL).

Appendix A. Supplementary data

Supplementary data to this article can be found online at https://doi.org/10.1016/j.soilbio.2022.108803.

References

Adair, E.C., Parton, W.J., Del Grosso, S.J., Silver, W.L., Harmon, M.E., Hall, S.A., Burke, I. C., Hart, S.C., 2008. Simple three-pool model accurately describes patterns of long-term litter decomposition in diverse climates. Global Change Biology 14, 2636–2660.

Adani, F., Spagnol, M., Nierop, K.G.J., 2007. Biochemical origin and refractory properties of humic acid extracted from maize plants: the contribution of lignin. Biogeochemistry 82, 55–65.

Akaike, H., 1974. A new look at the statistical model identification. IEEE Transactions on Automatic Control 19, 716–723.

Allison, S.D., Wallenstein, M.D., Bradford, M.A., 2010. Soil-carbon response to warming dependent on microbial physiology. Nature Geoscience 3, 336–340.

Amelung, W., Brodowski, S., Sandhage-Hofmann, A., Bol, R., 2008. Chapter 6: combining biomarker with stable isotope analyses for assessing the transformation and turnover of soil organic matter. Advances in Agronomy 100, 155–250.

Angst, G., Mueller, K.E., Kögel-Knabner, I., Freeman, K.H., Mueller, C.W., 2017. Aggregation controls the stability of lignin and lipids in clay-sized particulate and mineral associated organic matter. Biogeochemistry 132, 307–324.

Bahri, H., Rasse, D.P., Rumpel, C., Dignac, M.F., Bardoux, G., Mariotti, A., 2008. Lignin degradation during a laboratory incubation followed by 13C isotope analysis. Soil Biology and Biochemistry 40, 1916–1922.

Boerjan, W., Ralph, J., Baucher, M., 2003. Lignin biosynthesis. Annual Review of Plant Biology 54, 519–546.

Bondeau, A., Smith, P.C., Zaehle, S., Schaphoff, S., Lucht, W., Cramer, W., Gerten, D., Lotze-Campen, H., MÜLler, C., Reichstein, M., Smith, B., 2007. Modelling the role of agriculture for the 20th century global terrestrial carbon balance. Global Change Biology 13, 679–706.

Burnham, K.P., Anderson, D.R., 2004. Multimodel Inference: understanding AIC and BIC in model selection. Sociological Methods & Research 33, 261–304.

Cai, A., Liang, G., Zhang, X., Zhang, W., Li, L., Rui, Y., Xu, M., Luo, Y., 2018. Long-term straw decomposition in agro-ecosystems described by a unified three-exponentiation equation with thermal time. Science of the Total Environment 636, 699–708.

Calabrese, S., Porporato, A., 2019. Impact of ecohydrological fluctuations on iron-redox cycling. Soil Biology and Biochemistry 133, 188–195.

Chen, C., Hall, S.J., Coward, E., Thompson, A., 2020. Iron-mediated organic matter decomposition in humid soils can counteract protection. Nature Communications 11, 2255.

Chen, C., Meile, C., Wilmoth, J., Barcellos, D., Thompson, A., 2018. Influence of pO2 on iron redox cycling and anaerobic organic carbon mineralization in a humid tropical forest soil. Environmental Science and Technology 52, 7709–7719.

Clark, D.B., Mercado, L.M., Sitch, S., Jones, C.D., Gedney, N., Best, M.J., Pryor, M., Rooney, G.G., Essery, R.L.H., Blyth, E., Boucher, O., Harding, R.J., Huntingford, C., Cox, P.M., 2011. The Joint UK Land Environment Simulator (JULES), model description – Part 2: carbon fluxes and vegetation dynamics. Geoscientific Model Development 4, 701–722.

Córdova, S.C., Olk, D.C., Dietzel, R.N., Mueller, K.E., Archontouilis, S.V., Castellano, M. J., 2018. Plant litter quality affects the accumulation rate, composition, and stability of mineral-associated soil organic matter. Soil Biology and Biochemistry 125, 115–124.

Cotrufo, M.F., Soong, J.L., Horton, A.J., Campbell, E.E., Haddix, Michelle L., Wall, D.H., Parton, W.J., 2015. Formation of soil organic matter via biochemical and physical pathways of litter mass loss. Nature Geoscience 8, 776–779.

Cotrufo, M.F., Wallenstein, M.D., Boot, C.M., Denef, K., Paul, E., 2013. The Microbial Efficiency-Matrix Stabilization (MEMS) framework integrates plant litter decomposition with soil organic matter stabilization: do labile plant inputs form stable soil organic matter? Global Change Biology 19, 988–995.

Coward, E.K., Ohno, T., Plante, A.F., 2018. Adsorption and molecular fractionation of dissolved organic matter on iron-bearing mineral matrices of varying crystallinity. Environmental Science and Technology 52, 1036–1044.

Coward, E.K., Thompson, A.T., Plante, A.F., 2017. Iron-mediated mineralogical control of organic matter accumulation in tropical soils. Geoderma 306, 206–216.

Fang, K., Qin, S., Chen, L., Zhang, Q., Yang, Y., 2019. Al/Fe mineral controls on soil organic carbon stock across Tibetan alpine grasslands. Journal of Geophysical Research: Biogeosciences 124, 247–259.

Gelman, A., Rubin, D.B., 1992. Inference from iterative simulation using multiple sequences. Statistical Science 7, 457–511.

Ginn, B., Meile, C., Wilmoth, J., Tang, Y., Thompson, A., 2017. Rapid iron reduction rates are stimulated by high-amplitude redox fluctuations in a tropical forest soil. Environmental Science and Technology 51, 3250–3259.

Haario, H., Saksman, E., Tamminen, J., 2001. An adaptive Metropolis algorithm. Bernoulli 7, 223–242.

Hall, S.J., Huang, W., Timokhin, V.I., Hammel, K.E., 2020. Lignin Lags, Leads, or Limits the Decomposition of Litter and Soil Organic Carbon, vol. 101. Ecological Society of America.

Hall, S.J., Silver, W.L., 2013. Iron oxidation stimulates organic matter decomposition in humid tropical forest soils. Global Change Biology 19, 2804–2813.

Hall, S.J., Silver, W.L., Timokhin, V.I., Hammel, K.E., 2015. Lignin decomposition is sustained under fluctuating redox conditions in humid tropical forest soils. Global Change Biology 21, 2818–2828.

Hall, S.J., Silver, W.L., Timokhin, V.I., Hammel, K.E., 2016. Iron addition to soil specifically stabilized lignin. Soil Biology and Biochemistry 98, 95–98.

Hammel, K.E., Kapich, A.N., Jensen, K.A., Ryan, Z.C., 2002. Reactive oxygen species as agents of wood decay by fungi. Enzyme and Microbial Technology 30, 445–453.

Hararuk, O., Xia, J., Luo, Y., 2014. Evaluation and improvement of a global land model against soil carbon data using a Bayesian Markov chain Monte Carlo method. Journal of Geophysical Research: Biogeosciences 119, 403–417.

Hastings, W.K., 1970. Monte Carlo sampling methods using Markov chain and their applications. Biometrika 97–109.

Huang, W., Hammel, K.E., Hao, J., Thompson, A., Timokhin, V.I., Hall, S.J., 2019. Enrichment of lignin-derived carbon in mineral-associated soil organic matter. Environmental Science and Technology 53, 7522–7531.

Huang, W., Wang, K., Ye, C., Hockaday, W.C., Wang, G., Hall, S.J., 2021. High carbon losses from oxygen-limited soils challenge biogeochemical theory and model assumptions, 00 Global Change Biology 1–15.

Hyndman, R.J., Koehler, A.B., 2006. Another look at measures of forecast accuracy. International Journal of Forecasting 22, 679–688.

Izaurralde, R.C., Williams, J.R., McGill, W.B., Rosenberg, N.J., Jakas, M.C.Q., 2006. Simulating soil C dynamics with EPIC: model description and testing against long-term data. Ecological Modelling 192, 362–384.

Kallenbach, C.M., Frey, S.D., Grandy, A.S., 2016. Direct evidence for microbial-derived soil organic matter formation and its ecophysiological controls. Nature Communications 7, 13630.

Keiluweit, M., Wanzek, T., Kleber, M., Nico, P., Fendorf, S., 2017. Anaerobic microsites have an unaccounted role in soil carbon stabilization. Nature Communications 8, 1771.

Kirk, T.K., Farrell, R.L., 1987. Enzymatic "combustion": the microbial degradation of lignin. Annual Review of Microbiology 41, 465–505.

Kleber, M., 2010. What is recalcitrant soil organic matter? Environmental Chemistry 7.

Kleber, M., Eusterhues, K., Keiluweit, M., Mikutta, C., Mikutta, R., Nico, P.S., 2015. Mineral–organic associations: formation, properties, and relevance in soil environments. Advances in Agronomy 130, 1-140.

Koven, C.D., Riley, W.J., Subin, Z.M., Tang, J.Y., Torn, M.S., Collins, W.D., Bonan, G.B., Lawrence, D.M., Swenson, S.C., 2013. The effect of vertically resolved soil biogeochemistry and alternate soil C and N models on C dynamics of CLM4. Biogeosciences 10, 7109–7131.

Kramer, M.G., Sanderman, J., Chadwick, O.A., Chorover, J., Vitousek, P.M., 2012. Long-term carbon storage through retention of dissolved aromatic acids by reactive particles in soil. Global Change Biology 18, 2594–2605.

Lalonde, K., Mucci, A., Ouellet, A., Gelinas, Y., 2012. Preservation of organic matter in sediments promoted by iron. Nature 483, 198–200.

Liang, J., Li, D., Shi, Z., Tiedje, J.M., Zhou, J., Schuur, E.A.G., Konstantinidis, K.T., Luo, Y., 2015. Methods for estimating temperature sensitivity of soil organic matter based on incubation data: a comparative evaluation. Soil Biology and Biochemistry 80, 127–135.

Luo, Y., Melillo, J., Niu, S., Beier, C., Clark, J.S., Classen, A.T., Davidson, E., Dukes, J.S., Evans, R.D., Field, C.B., Czimczik, C.I., Keller, M., Kimball, B.A., Kueppers, L.M., Norby, R.J., Pelini, S.L., Pendall, E., Rastetter, E., Six, J., Smith, M., Tjoelker, M.G., Torn, M.S., 2011. Coordinated approaches to quantify long-term ecosystem dynamics in response to global change. Global Change Biology 17, 843–854.

Luo, Y., Smith, B., 2022. Land Carbon Cycle Modeling: Matrix Approach, Data Assimilation, & Ecological Forecasting. CPC Press, Taylor & Francis Group.

Luo, Y., White, L.W., Canadell, J.G., DeLucia, E.H., Ellsworth, D.S., Finzi, A., Lichter, J., Schlesinger, W.H., 2003. Sustainability of terrestrial carbon sequestration: a case study in Duke Forest with inversion approach. Global Biogeochemical Cycles 17.

Lützow, M.v., Kögel-Knabner, I., Ekschmitt, K., Matzner, E., Guggenberger, G., Marschner, B., Flessa, H., 2006. Stabilization of organic matter in temperate soils: mechanisms and their relevance under different soil conditions - a review. European Journal of Soil Science 57, 426–445.

Martin, J.P., Haider, K., Kassim, G., 1980. Biodegradation and stabilization after 2 Years of specific crop, lignin, and polysaccharide carbons in soils. Soil Science Society of America Journal 44, 1250.

McKendrick, A.G., Pai, M.K., 1911. The rate of multiplication of micro-organisms: a mathematical study. proceedings of the Royal Society of Edinburgh 31, 649–655.

Metropolis, N., Rosenbluth, A.W., Rosenbluth, M.N., Teller, A.H., Teller, E., 1953. Equation of state calculations by fast computing machines. The Journal of Chemical Physics 21, 1087–1092.

Miltner, A., Bombach, P., Schmidt-Brücken, B., Kästner, M., 2011. SOM genesis: microbial biomass as a significant source. Biogeochemistry 111, 41–55.

Monod, J., 1949. The growth of bacterial cultures. Annual review 3, 371–394.

Parton, W.J., Schimel, D.S., Cole, C.V., Ojima, D.S., 1987. Analysis of factors controlling soil organic matter levels in great plains grasslands. Soil Science Society of America Journal 51, 1173–1179.

Parton, W.J., Scurlock, J.M.O., Ojima, D.S., Gilmanov, T.G., Scholens, R.J., Schimel, D.S., Kirchner, T., Menaut, J.-C., Seastedt, T., Moya, E.G., Kamnalrut, A., Kinyamaro, J.I., 1993. Observations and modeling of biomass and soil organic matter dynamics for the grassland biome worldwide. Global Biogeochemical Cycles 7, 785–809.

Riedel, T., Zak, D., Biester, H., Dittmar, T., 2013. Iron traps terrestrially derived dissolved organic matter at redox interfaces. Proceedings of the National Academy of Sciences of the United States of America 110, 10101–10105.

Schadel, C., Schuur, E.A., Bracho, R., Elberling, B., Knoblauch, C., Lee, H., Luo, Y., Shaver, G.R., Turetsky, M.R., 2014. Circumpolar assessment of permafrost C quality and its vulnerability over time using long-term incubation data. Global Change Biology 20, 641–652.

Schimel, J., Weintraub, M.N., 2003. The implications of exoenzyme activity on microbial carbon and nitrogen limitation in soil: a theoretical model. Soil Biology and Biochemistry 35, 549–563.

Schmidt, M.W., Torn, M.S., Abiven, S., Dittmar, T., Guggenberger, G., Janssens, I.A., Kleber, M., Kogel-Knabner, I., Lehmann, J., Manning, D.A., Nannipieri, P., Rasse, D. P., Weiner, S., Trumbore, S.E., 2011. Persistence of soil organic matter as an ecosystem property. Nature 478, 49–56.

Talbot, J.M., Treseder, K.K., 2012. Interactions among lignin, cellulose, and nitrogen drive litter chemistry–decay relationships. Ecological Society of America 93, 345–354.

Tao, F., Zhou, Z., Huang, Y., Li, Q., Lu, X., Ma, S., Huang, X., Liang, Y., Hugelius, G., Jiang, L., Doughty, R., Ren, Z., Luo, Y., 2020. Deep learning optimizes data-driven representation of soil organic carbon in earth system model over the conterminous United States. Frontiers in Big Data 3.

Thevenot, M., Dignac, M.-F., Rumpel, C., 2010. Fate of lignins in soils: a review. Soil Biology and Biochemistry 42, 1200–1211.

Wang, Y.P., Chen, B.C., Wieder, W.R., Leite, M., Medlyn, B.E., Rasmussen, M., Smith, M. J., Agusto, F.B., Hoffman, F., Luo, Y.Q., 2014. Oscillatory behavior of two nonlinear microbial models of soil carbon decomposition. Biogeosciences 11, 1817–1831.

Weber, K.A., Achenbach, L.A., Coates, J.D., 2006. Microorganisms pumping iron: anaerobic microbial iron oxidation and reduction. Nature Reviews Microbiology 4, 752–764.

Wieder, W.R., Bonan, G.B., Allison, S.D., 2013. Global soil carbon projections are improved by modelling microbial processes. Nature Climate Change 3, 909–912.

Winkler, P., Kaiser, K., Thompson, A., Kalbitz, K., Fiedler, S., Jahn, R., 2018. Contrasting evolution of iron phase composition in soils exposed to redox fluctuations. Geochimica et Cosmochimica Acta 235, 89–102.

Wood, P.M., 1994. Pathways for production of Fenton's reagent by wood-rotting fungi. Federation of European Microbiological Societies 13, 313–320.

Woolf, D., Lehmann, J., 2019. Microbial models with minimal mineral protection can explain long-term soil organic carbon persistence. Scientifc Reports 9, 6522.

Xu, T., White, L., Hui, D., Luo, Y., 2006. Probabilistic inversion of a terrestrial ecosystem model: analysis of uncertainty in parameter estimation and model prediction. Global Biogeochemical Cycles 20, G2007.

Xu, X., Shi, Z., Li, D., Rey, A., Ruan, H., Craine, J.M., Liang, J., Zhou, J., Luo, Y., 2016. Soil properties control decomposition of soil organic carbon: results from data-assimilation analysis. Geoderma 262, 235–242.

Zhang, D., Hui, D., Luo, Y., Zhou, G., 2008. Rates of litter decomposition in terrestrial ecosystems: global patterns and controlling factors. Journal of Plant Ecology 1, 85–93.

Zhao, Q., Poulson, S.R., Obrist, D., Sumaila, S., Dynes, J.J., McBeth, J.M., Yang, Y., 2016. Iron-bound organic carbon in forest soils: quantification and characterization. Biogeosciences 13, 4777–4788.

Zheng, J., Thornton, P.E., Painter, S.L., Gu, B., Wullschleger, S.D., Graham, D.E., 2019. Modeling anaerobic soil organic carbon decomposition in Arctic polygon tundra: insights into soil geochemical influences on carbon mineralization. Biogeosciences 16, 663–680.